Ocean Engineering 239 (2021) 109837

Contents lists available at ScienceDirect

Ocean Engineering

journal homepage: www.elsevier.com/locate/oceaneng

# Design of an aeroelastic physical model of the DTU 10MW wind turbine for a floating offshore multipurpose platform prototype

S. Muggiasca [a,*], F. Taruffi [a], A. Fontanella [a], S. Di Carlo [a], H. Giberti [b], A. Facchinetti [a], M. Belloli [a]

[a] Department of Mechanical Engineering, Politecnico di Milano, Via La Masa 1, 20156, Milan, Italy
[b] Dipartimento di ingegneria industriale e Dell'informazione. Università di Pavia, Via ferrata 5, 27100, Pavia, Italy

ARTICLE INFO

*Keywords:*
Offshore platform
Multi-function platform
FOWT
Aeroelastic model
Wind energy
Blade design

ABSTRACT

Multi-purpose offshore structures are very complex systems to be designed as many different requirements have to be taken into account simultaneously. Experimental tests on scaled models can be very useful to verify structural behavior and to validate numerical models. The definition of the scale can play a key role in performing tests as high scales, closer to full-scale, are generally related to more reliable results. The present paper concerns the design of a wind turbine model for a large-scale model of a Multi-purpose offshore Platform developed within the EU project H2020 Blue Growth Farm. This project aims at developing an offshore farm, based on a modular floating structure that integrates wave energy converters and a wind turbine with aquaculture. The scale model of the complete structure will be deployed at the Natural Ocean Engineering Laboratory (NOEL). The paper will focus on the strategies adopted to scale 1:15 the DTU 10 MW wind turbine in order to represent both the main aeroelastic features and all the functionalities of a real machine. The complete design of the machine and its control will be also provided.

## 1. Introduction

Floating Offshore Wind Turbines (FOWTs) are recognized both by industry and academia as the key technology to exploit the high-quality wind resource of waters deeper than 50 m. One interesting possibility offered by FOWTs is that the floating platform required to support the wind turbine can be exploited for other purposes related to the marine environment. Multi-Purpose-Platform (MPP) is a promising concept in ocean engineering as it enables more efficient space usage and to share infrastructures, thus saving costs. Until now different kinds of MPP have been proposed (Nassar et al., 2020; Pérez-Collazo et al., 2015; Pernice, 2009), grouping different technologies and subsystems: great support, especially from the EU, is devoted to supporting the research in Blue Growth (Jouffray et al., 2020). In this scenario, The Blue Growth Farm project (EU H2020) has the objective to develop a Multi-purpose offshore farm. The farm is placed on a modular floating structure and its targets are efficiency, cost-competitiveness and environmental-friendliness. A wind turbine is combined with wave energy converters and aquaculture to achieve cost-effectiveness in various high-sea applications.

Experimental data are required to support the design procedure adopted for commercial FOWTs in order to cope with the increased complexity of the multi-purpose floating system: the research has a key role in the development of offshore technology related to wind turbine applications and it is even more important in improving the knowledge for a complex system as MPP that collects different subsystem, each one with its peculiarities. Experimental activities for a single floating system are generally performed on scale models on wind tunnel or in wave basin: the indoor tests are generally performed using a low scale factor (about 100), reaching a Technology Readiness Level (TRL) of about 3–5. For MPP, due to their complexity, tests in indoor laboratories are not considered sufficient for a proper design. Further intermediate steps between small-scale indoor experiments and prototypal activities are required. An intermediate-scale outdoor activity permits to reach higher scale factors ($\lambda_L < 30$) and higher TRLs (about 5–7). Outdoor tests can be very challenging due to the uncontrolled environmental conditions that do not allow for simulations of simple wind and wave inputs: the design of the scale model has to deal with the probabilistic distribution of wind and wave in the considered site. On the other hand, a reduction of the scale effects is expected and the possibility to perform long time scale tests can be very useful to investigate low-frequency dynamic effects and

* Corresponding author.
*E-mail address:* sara.muggiasca@polimi.it (S. Muggiasca).

https://doi.org/10.1016/j.oceaneng.2021.109837
Received 29 February 2020; Received in revised form 9 August 2021; Accepted 10 September 2021
Available online 27 September 2021

**Nomenclature**

| | |
|---|---|
| RWT | Reference Wind Turbine |
| FOWT | Floating Offshore Wind Turbine |
| TSR | Tip Speed Ratio |
| TRL | Technology Readiness Level |
| MPP | Multi-Purpose-Platform |
| OSP | Outdoor Scaled Prototype |
| U [m/s] | Hub-height horizontal wind speed |
| g [m/s$^2$] | Gravity acceleration |
| $U_{10min}$ [m/s] | 10-min mean wind speed |
| Fr=U/$\sqrt{gL}$ | Froude Number |
| Re=UL/$\nu$ | Reynolds Number |
| $\nu$ [m$^2$/s] | Kinematic air viscosity |
| t [m] | Airfoil thickness |
| c [m] | Chord length |
| $C_L$ [-] | Lift coefficient |
| AoA [deg] | Angle of Attack. |
| E [N/m$^2$] | Young's modulus |
| EJ [N m$^2$] | Bending stiffness |

perform probabilistic analysis of the MPP behaviour. Within The Blue Growth Farm project an Outdoor Scaled Prototype (OSP), characterized by a scale of 1:15, was designed and the location of the Natural Ocean Engineering Laboratory (NOEL) in Reggio Calabria was judged appropriate for the tests. The Reference Wind Turbine (RWT) adopted for this application is the DTU 10 MW. The present work focuses on the design of the wind turbine for the OSP, highlighting the main challenges related to the large scale required and the uncontrolled testing environment. As well as for the indoor tests, the wind turbine must be scaled considering its aeroelastic characteristics as a structure and its functionalities as a machine. On the other hand, differently from small-scale models, safety issues must be taken into account in order to grant a proper behaviour of the wind turbine even under extreme wind and wave events. Moreover, further functionalities have to be implemented as the control of the alignment between the turbine axis and the wind. Even the power controller must consider all the possible scenarios related to a real wind turbine functioning. In the end, the design of a wind turbine for a large MPP model for outdoor tests can be considered as the result of a compromise between a scale model and a real turbine design.

In Section 2 the scaling procedure is presented highlighting the strategies adopted to scale in an aeroelastic way the tower, and for the aerodynamic design of the rotor. In Section 3 the structural design of all the components is reported describing both the mechatronic design of the nacelle and the assessment of the main structural components. In Section 4 the control strategies are described. Further information about the platform and the related OSP design can be found in Li et al., (2019), Ruzzo et al., 2019. The mutual influence of the wind turbine and the platform is not reported in the paper, but it has been considered for the very final assessment of the model: numerical simulations and wave basin tests have been performed in order to simulate the dynamic behaviour of the MPP and they have been used to check the design of the OSP (Li et al., 2020).

## 2. Scaling procedure for the outdoor scaled prototype

### 2.1. o reference DTU 10 MW wind turbine

The wind turbine included in the full-scale project is the DTU 10 MW, which was first developed within the Light Rotor project in 2012 (Bak et al., 2012), upscaling the 5 MW NREL design (Jonkman et al., 2009).

The evolution of this model released by DTU is reported in Bak et al., (2013), and it is adopted in several current research activities related to wind energy development, with emphasis to offshore applications studies, and also for numerical tools benchmark and validation (Bayati et al., 2018a; Bayati et al., 2018b). Table 1 reports the main DTU 10 MW specifications in terms of dimensions, masses and operating wind speed.

**Table 1**
DTU 10 MW turbine specifications.

| | |
|---|---|
| Cut-in wind speed [m/s] | 4 |
| Cut-out wind speed [m/s] | 25 |
| Rated wind speed [m/s] | 11.4 |
| Rotor Diameter [m] | 178.3 |
| Hub Diameter [m] | 5.6 |
| Hub Height [m] | 119 |
| Minimum Rotor Speed [rpm] | 6 |
| Maximum Rotor Speed [rpm] | 9.6 |
| Blade Prebend [m] | 3.332 |
| Rotor Mass [t] | 228 |
| Nacelle Mass [t] | 446 |
| Tower Mass [t] | 628.4 |

### 2.2. General scaling strategies

The wind turbine for OSP represents a challenging project that has to satisfy, at the same time, the requirements of a classic aeroelastic scale model and of a real small-scale wind turbine. This means to adopt, together with the typical procedures used to design an aeroelastic model, additional strategies in order to grant the main functionalities of the full-scale wind turbine and to realize a safe structural design. Generally, to realize a scale model for offshore applications, Froude-similitude is required, because it enables the correct reproduction of gravity-dependent loads (e.g. weight and waves). Froude-similitude is obtained imposing the same Fr for the scale model and the full-scale system. For the OSP design, a compromise between this scaling rule and the requirements related to the interaction between the prototype and the real-life environment in the laboratory area must be considered. In particular, as explained in detail in section 2.3, the aerodynamics was scaled following the Froude law only in terms of thrust force that, together with hydrodynamics and weight, is one of the actions that mostly affect the wind turbine dynamics. For the definition of the operating conditions, other strategies were used to take into account the peculiarities of a natural laboratory. As anticipated, experiments will be

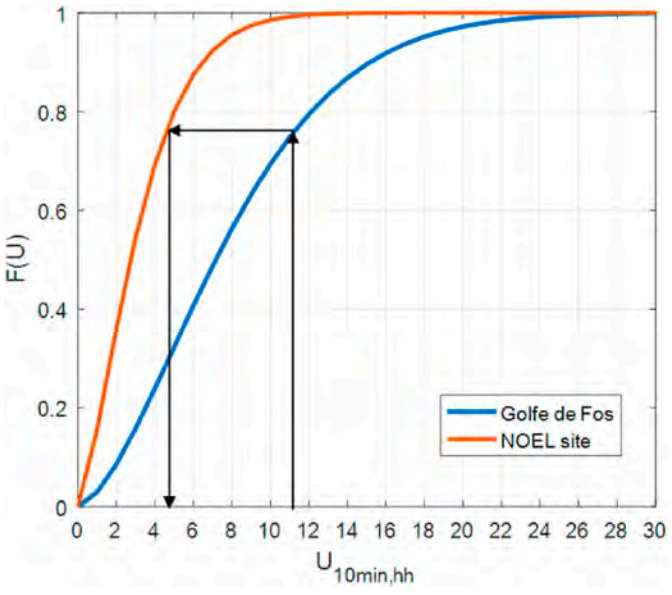


**Fig. 1.** Cumulative distribution functions of the wind velocities for Golfe de Fos and NOEL site.

**Table 2**
Scaling parameters.

| Length scale | $\lambda_L$ | 15 |
|---|---|---|
| Length ratio (no Froude) | $D^R_{rotor}/D^M_{rotor}$ | 26 |
| Velocity ratio (no Froude) | $\lambda_V$ | 2.28 |
| Mass scale | $\lambda_M = \lambda_L^3$ | 3375 |
| Moment of inertia scale | $\lambda_J = \lambda_L^5$ | 759375 |
| Force scale | $\lambda_F = \lambda_L^3$ | 3375 |
| Frequency ratio (no Froude) | $\omega^R_{rotor}/\omega^M_{rotor}$ | 0.09 |

performed in the NOEL site, a natural laboratory whose metocean conditions are a scaled representation of typical FOWT deployment sites. Unlike traditional indoor laboratory tests in a wind tunnel or in an ocean basin, the wind and waves cannot be controlled, and the experimental conditions must be considered in the model design process based on a probabilistic approach. Moreover, as the interdependence of wind and waves at NOEL might not be representative of the target FOWT deployment sites, a compromise in defining the scaling parameters for hydrodynamic and aerodynamic phenomena must be found. Between the possible deployment sites, Golfe de Fos was chosen as a reference: this area is located in Southern France at about 30–40 km offshore of Fos sur Mer, in the region of Provence-Alpes-Côte d'Azur. The site, already considered in the EU H2020 LIFE50+ project, was judged suitable also within the BGF project, as its met-ocean conditions can be scaled at NOEL using a length scale within the range 1:10–1:20 (for a complete database of Golfe de Fos met-ocean data see Gómez et al., 2015 and Krieger et al., 2015).

In order to define the wind speed scale factor, the cumulative distribution functions of wind speed for the Golfe de Fos and the NOEL laboratory were compared (see Fig. 1): the rated wind speed at NOEL was fixed at about 5 m/s, a value that shows a similar probability of exceedance to the full-scale Rated wind speed (11.4 m/s) at Golfe de Fos (see the arrows reported in Fig. 1). This criterion seemed to be reasonable to grant the occurrence of the operating conditions for the wind turbine during the experimental campaign, ensuring the same probability to have the wind turbine working in partial or full-load conditions for the model and the full-scale system. This wind velocity was also judged as a proper dimensioning value for structural issues.

The length scale ratio was fixed to 1:15. This value was obtained by comparing the dimensions of the full-scale system and the NOEL laboratory. Economic and social factors were also taken into account, considering that limiting the maximum prototype dimensions allows controlling costs, facilitating the model installation and promoting the community acceptance of a quite large structure placed in the close-shore location of the laboratory. Once the length scale factor was defined, the other parameters were at first defined applying the Froude scaling approach, with particular reference to the thrust force acting on the rotor, the masses and the tower aeroelastic parameters (see Table 2). The scaling of these quantities following the Froude law permitted to properly reproduce, in scale, the phenomena where gravity and inertial forces are dominant. As highlighted by Robertson et al., (2013), to scale the rotor, the shape of the blade must be re-designed as a simple geometrical scaling would not permit to obtain the same performances of the RWT due to the difference in Re between prototype and full-scale: the Re range for the prototype is expected to be of the order of $10^5$ while the Re for the RWT was about $10^7$. The so-called "performance scaling" (De Ridder et al., 2014; Bayati et al., 2017a Bayati et al., 2017b) must be applied. This consists in redesigning the blade geometry in order to obtain the scaled thrust force, at the scaled wind speed. In particular, an airfoil for the prototype blade which is able to show a lift coefficient with a linear trend as a function of the AoA, far from the stall conditions, at Re of the operating wind turbine conditions, must be selected. The performance scaling was applied considering as target the thrust force scaled by Froude law and the wind speed used to define the wind turbine

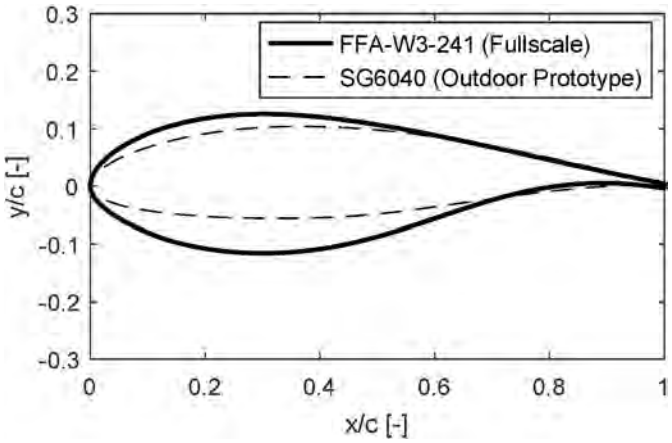


**Fig. 2.** Model airfoil (SG6040, dashed line) and reference airfoil (FFA-W3-240, solid line).

operating conditions, scaled using the adopted non-Froude velocity scale ratio. A more detailed description of the rotor design is provided in the next section 'Rotor scaling process'. Finally, concerning the nacelle scaling, the Froude approach was used to define the global mass and the overall dimensions, while the functionality requirements are considered for the complete design. Further details will be provided in the 'Nacelle scaling process' section. The main scaling factors used in the model design are summarized in Table 2.

### 2.3. Rotor scaling process

The "performance scaling" procedure was applied to properly scale the rotor, in agreement with the procedure described in Bayati et al., 2017a), with some differences in consideration of the peculiarities of the present application. Differently from the procedure described in Bayati et al., 2017a), aerodynamic and structural optimizations were performed separately, using FE analysis for the structural design. Other modifications were brought because geometry and velocity scale factors were defined independently as described in the previous section. Moreover, a further constraint was imposed, assigning a maximum rotor diameter of 10 m, in agreement with the policies adopted to limit the maximum dimensions of the OSP. The global effect of all the implemented design strategies resulted in a scale factor for the rotor, named

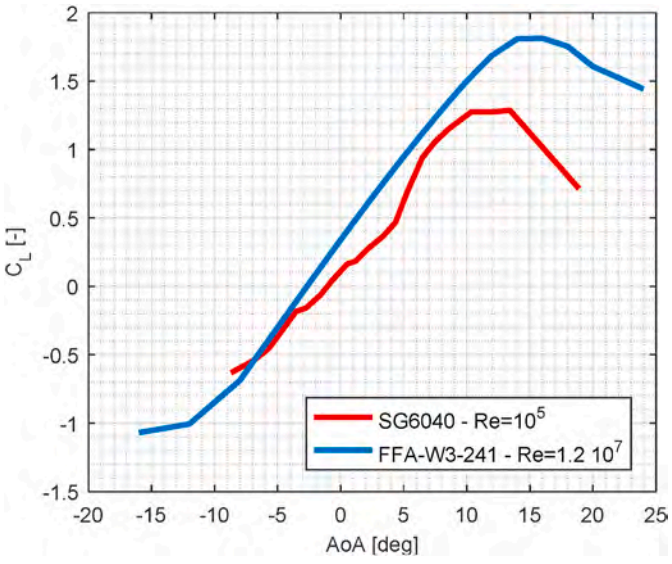


**Fig. 3.** Reference and model airfoil lift coefficient comparison.

**Fig. 4.** SG6040 2D section model inside the wind tunnel.

the length ratio, of 1:26 (see Table 2), which is different than the scale factor for any other component of the OSP. The high number of constraints encountered in the design of the OSP blades imposes compromises giving priority to the reproduction of the thrust force, the scaling of the masses and the safety issues; less importance was attributed to the blade aeroelastic characteristics, differently to the procedure described in Bayati et al., 2017a). The aerodynamic design procedure was divided into two main steps, the first focused on the 2D geometry, the second on the 3D geometry. The first step imposed the selection of an airfoil suitable for the Re of the prototype i.e. the local Re evaluated considering the TSR and the wind velocity for the OSP at Rated condition: in Lyon et al., 1998) a wide database of airfoil shapes optimized for low Re conditions is provided. For the present project, the SG6040 profile was chosen as it shows an intermediate value of thickness over chord length ratio (16%) suitable in low Re conditions to avoid flow separation, and able, at the same time, to grant good structural performances compared to the expected loads. In Fig. 2 the selected profile is compared to one of the DTU 10 MW airfoils.

The SG6040 profile also shows an aerodynamic behaviour suitable for wind turbines having a lift coefficient curve characterized by a linear trend for a wide range of AoA, which permits to keep the wind turbine operating far from the stall (see Fig. 3). The operating conditions for the OSP are defined by scaling the cut-in and the cut-out wind speeds of the RWT (see Table 1) by the non-Froude velocity scale factor resulting in the range 1.75–11 m/s.

The lift coefficient data reported in literature for SG6040 profile were verified through 2D wind tunnel tests, at the Re expected for the wind turbine prototype and the results are reported in the following section. In particular, combining the velocity of the incoming wind and the blade rotating velocity and considering the chord expected variation along the blade, the Re at the Rated for the OSP is between $0.5{\cdot}10^5$ (at the blade root) and $1.6{\cdot}10^5$.

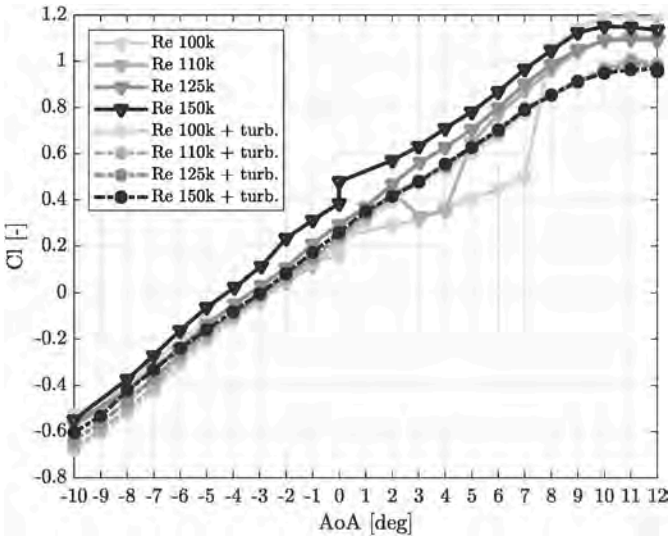


**Fig. 5.** Lift coefficient of the SG6040 airfoil measured from 2D section model wind tunnel tests for different Re without added turbulence and with added turbulence (+turb.).

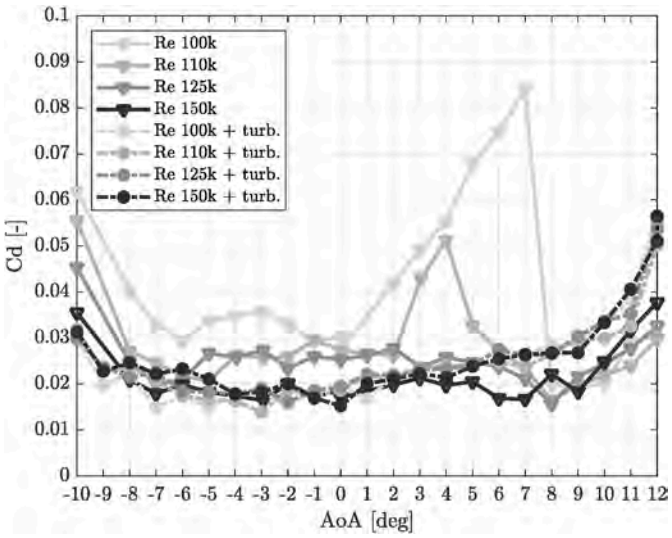


**Fig. 6.** Drag coefficient of the SG6040 airfoil measured from 2D section model wind tunnel tests for different Re without added turbulence and with added turbulence (+turb.).

### 2.3.1. 2D wind tunnel tests

The input for the performance scaling procedure is the set of aerodynamic coefficients of the selected airfoil. Any uncertainty in the aerodynamic coefficients may impact the capability of the designed rotor of reproducing the behaviour of the target full-scale rotor. Defining the aerodynamic coefficients for low-speed airfoils like the SG6040 is often difficult. The flow over airfoils at low Re is complex because phenomena like laminar separation and transition to turbulent flow are often present (Guglielmo and Selig, 1996). The aerodynamic coefficients for the SG6040 are tabled in Lyon et al., (1998) for Re $1{\cdot}10^5$, $1.5{\cdot}10^5$, $2{\cdot}10^5$, $3{\cdot}10^5$, $4{\cdot}10^5$ and $5{\cdot}10^5$. Because of the sensitivity of aerodynamic coefficients to parameters like Re, freestream turbulence and surface roughness of the profile, it was decided to carry out a dedicated series of wind tunnel tests to measure the aerodynamic coefficients of the SG6040. Experiments were carried out at the Politecnico di Milano De

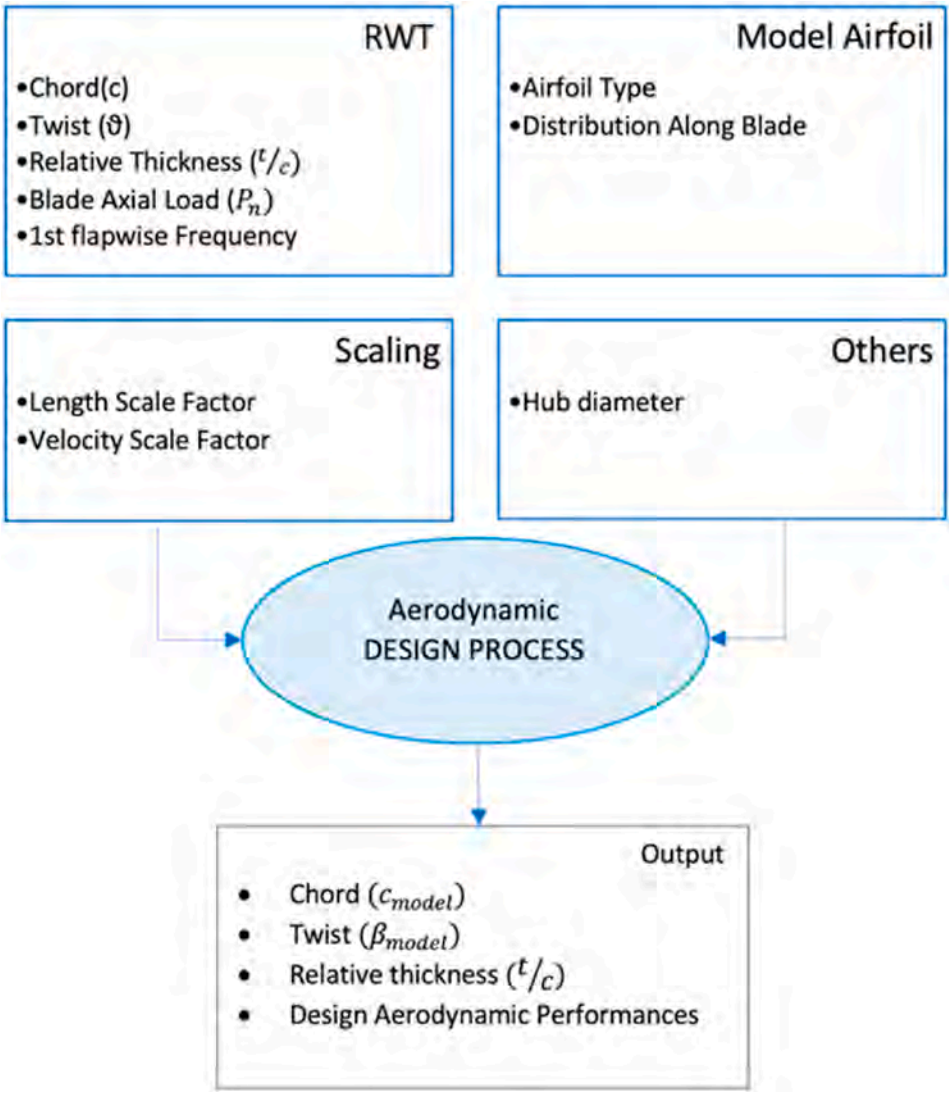


**Fig. 7.** Design code scheme.

Ponte wind tunnel on a 2D section model (see Fig. 4). This was manufactured in carbon fiber reinforced plastic as the scale model blade to have a similar surface roughness. The model is 920 mm span-wise long and 200 mm chord-wise long. Two aerodynamic coefficients were measured. The lift coefficient was measured from 32 pressure taps directly drilled on the surface of the model central section (10 mm span-wise). The drag coefficient was obtained from the wake momentum. Pressure data were acquired by a wake rake placed downstream of the model at a distance of 20% from the trailing edge in correspondence of its central section. Aerodynamic coefficients were measured for Re related to the Rated conditions for the OSP, $1{\cdot}10^5$, $1.1{\cdot}10^5$, $1.25{\cdot}10^5$and $1.5{\cdot}10^5$in smooth flow (index of turbulence lower than 0.5%) and increasing the freestream turbulence level to a minimum value expected for the wind turbine model in operation (index of turbulence ≈ 1.5%). The measured aerodynamic coefficients are reported in Fig. 5 and Fig. 6. The great increase in drag coefficient for Re $1{\cdot}10^5$-$1.1{\cdot}10^5$ highlights the formation of a separation bubble typical for low-speed airfoils (Guglielmo and Selig, 1996). This effect does not appear when the freestream turbulence is increased.

### 2.3.2. Final aerodynamic design

The 3D design of the blade includes the evaluation of the chord and twist, main characteristics of the blade in terms of geometry in order to reach the target thrust. A general overview of this process is given in the block diagram of Fig. 7. The script takes as input the full-scale chord, twist and thickness distribution, together with the force coefficients of the RWT airfoils. Based on the theoretical considerations of the thrust matching strategy, the code computes at each iteration the optimal chord and twist distributions to match the thrust force on the rotor.

The first step is a comparison between the lift curves of the SG6040 airfoil at the appropriate Re and the ones of the full-scale profile. At Rated wind speed, the Re is evaluated and for the sake of simplicity, the presence of the induction factors is neglected:

$$V_{rel}(r) = \sqrt{(\Omega\%(r_{nub} + r))^2 + U_\infty^2} \tag{1}$$

$$\mathrm{Re}(r) = \frac{pV_{rel}(r)c(r)}{\mu} \tag{2}$$

where $(r_{hub} + r)$ is the distance between the rotor axis and the blade station and $c(r)$ is the chord of the local profile. A fixed Re for the full-scale profile is considered in this comparison. The linear regions of the two airfoils are isolated, the angular coefficients $(K_{L,DTU}, K_{L,model})$ and the y-axis intercepts $(C^0_{L,DTU}, C^0_{L,model})$ are calculated and used to scale the chord and correct the twist angle for each radial station (see Bayati et al., 2017a). From this design process, the chord and twist distribution of the

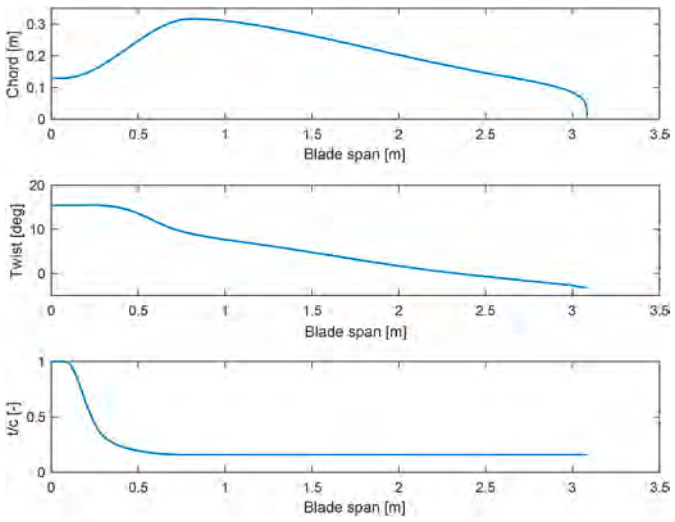


**Fig. 8.** Chord, twist and chord relative thickness value vs blade span.

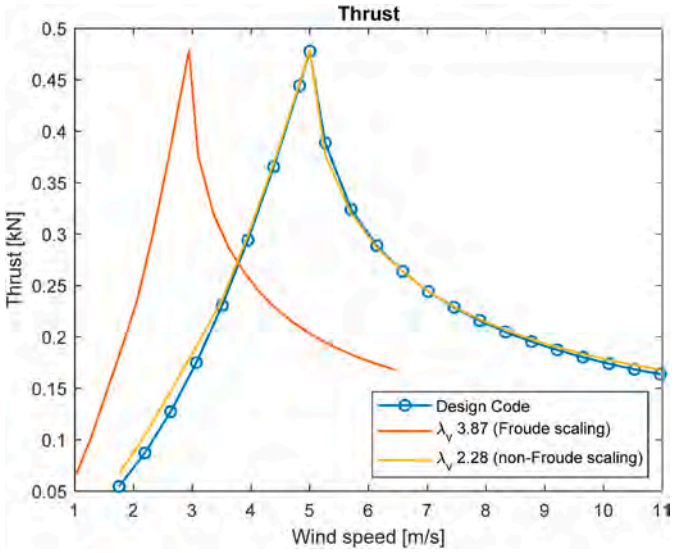


**Fig. 9.** Thrust for the overall working range.

scaled blade is determined. After all, the scaled thrust must still be achieved and a post-processing operation is required. The chord is the degree of freedom to play with, in order to allow variations of the thrust. The correction routine for the chord works using an iterative process realized through FAST v8.16 steady-state simulations. A rigid FAST model composed of 193 sections along the radial coordinate is generated: this model can be considered an acceptable approximation since in static tests the rotational speed of the turbine is constant, therefore the rotor performance is not affected by the inertial properties of the system. Then a chord correction is implemented and the input FAST files are modified so to start again with the thrust evaluation and comparison. Blade section profile is forced to vary with a third-order polynomial with null derivatives at the extremities to have a blade chord profile without edges from the circular section (hub) to the maximum chord cross-section. The results of the iterative process in terms of chord, twist and thickness distribution are reported in Fig. 8.

The results of the numerical simulations in terms of thrust force are compared in Fig. 9 to the reference values, obtained by scaling the RWT thrust force and scaling the wind velocity according to the selected non-Frude wind velocity scaling ratio: a good agreement between the two curves can be noticed.

A parametrized analysis was performed in FAST for different combinations of pitch angles, TSRs and wind velocities, to have an overview of the variation of the power and thrust coefficients in the possible operating conditions. A comparison between the prototype and the RWT is shown in Fig. 10 and similarities can be found almost for each operating condition even if the prototype performances result generally lower than the ones of the full-scale turbine.

The main parameters regarding the designed rotor are reported in Table 3.

### 2.4. Tower scaling process

The tower is the main structural component of the wind turbine because it supports the nacelle and the rotor assemblies providing the necessary elevation of the rotor to reach the level where the wind resources are. The prototype tower characteristics were defined scaling the RWT tower, with particular care to the stiffness and flexural frequencies that are scaled using Froude approach in order to obtain an aeroelastic model. Two possible solutions were considered at the beginning: a tower made of an aluminum or a steel tube (Fontanella et al., 2019; Muggiasca et al., 2019). The steel solution was preferred because it allows to easily satisfy stresses and buckling assessments and to simplify the design of the extremity connections. Moreover, it is easier to find a steel commercial tube suitable for the application. On the other hand, a great reduction of the outer tower diameter must be accepted: as the full-scale structure uses the same material, the elastic module E is fixed and in order to obtain the proper flexural stiffness EJ, the section dimensions cannot satisfy geometrical scaling. This compromise was judged acceptable especially considering that even by properly scaling the tower geometry, a strong discrepancy in terms of Reynolds number between prototype and full-scale tower would be observed.

As shown in Fig. 11, the tower of the designed prototype is in the subcritical region of the drag curve whereas the real tower is in the supercritical Re range. This difference results in a higher drag coefficient for the model and some differences in the flow-structure interaction. However, as highlighted in Belloli et al., (2015), the main fluid-dynamics features, especially the VIV characteristics, are similar for these two regions.

In Table 4 drag force at Rated wind velocity on the OSP is compared with the corresponding force referred to RWT and scaled 1:15: it is possible to note that the difference in drag coefficient is not compensated by the reduced diameter resulting in a higher value compared to the target. The drag force can be anyway considered negligible compared to other aerodynamic loads as the rotor thrust force (see Table 4 for the Rated wind velocity).

The frequencies values that have to be matched (from the DTU 10 MW RWT) are equal to 0.97 Hz both for the fore-aft and for the side-side mode. The frequencies of the OSP tower have been defined using FEM calculations and the obtained value for the two modes is 1.1 Hz. The obtained frequency is higher than the target one, but it is the best compromise between the objectives of matching the masses of the structure components, satisfying the structural resistance constraints, verifying the availability of standard dimensioned steel poles. Actually, even if the masses of Rotor and Nacelle are higher than the target (see Table 6), the natural frequency of the first mode of the tower is higher due to the increased bending stiffness of the chosen steel pole. A strategy to decrease the frequency would be to add mass on the top of the tower, but this approach would increase the error on the Rotor and Nacelle masses scaling. The modal shape was also considered: the comparison between RWT and OSP is reported in Fig. 12 where a good agreement is observed (the axis values are normalized in order to compare the modal shapes of towers having different heights).

The main characteristics of the prototype tower are reported in Table 5.

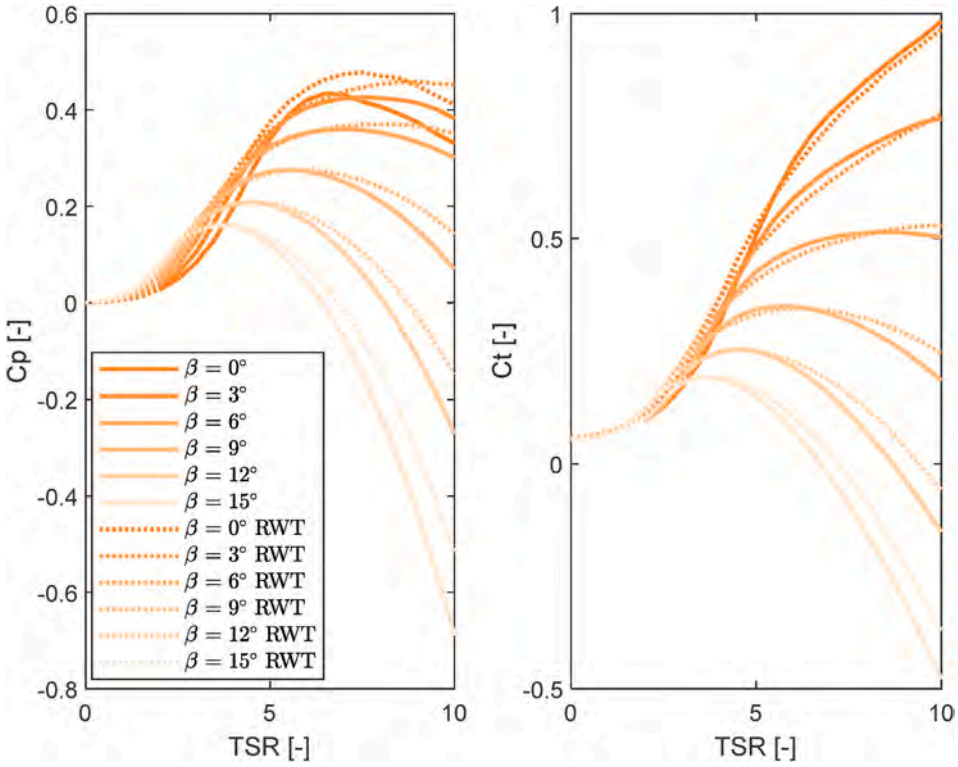


**Fig. 10.** Power ($C_p$) and thrust ($C_t$) coefficients for RWT (dotted) and for the OSP (solid) for different pitch angles β and tip-speed ratios (TSR).

**Table 3**
Main rotor parameters.

| | | |
|---|---|---|
| Geometric scale factor for the rotor | $D^R_{rotor}/D^M_{rotor}$ | 26 |
| Velocity ratio (no Froude) | $\lambda_V$ | 2.28 |
| Tip speed Ratio | | 7.5 |
| Hub radius | | 0.345 |
| Diameter of the root circular section | | 0.13 |
| Extension of the cylindrical part of the blade | | 0.07 |
| Extension of the transition zone (from cylindrical section to SG6040) | $l_{tip}$ [m] | 0.7984 |
| Length of the blade | $l_{blade}$ [m] | 3.085 |
| Rotor radius | $r_{rotor}$ [m] | 3.4288 |
| Cut-in wind speed | $U_{cutin}$[m/s] | 1.75 |
| Cut-out wind speed | $U_{cutout}$[m/s] | 11 |
| Rated wind speed | $U_{rated}$[m/s] | 5 |
| Rated RPM | $\Omega_{rated}$ [rpm] | 109.474 |

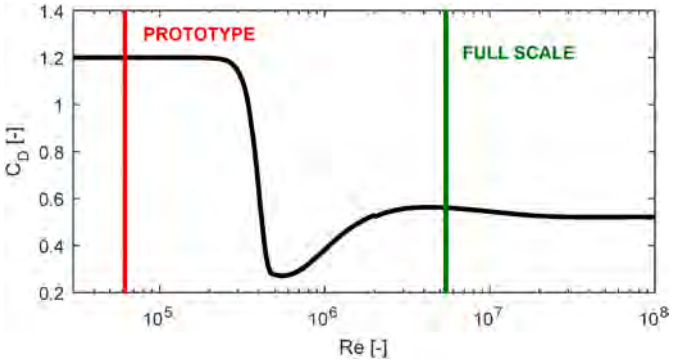


**Fig. 11.** Drag coefficient of a smooth circular cylinder as a function of Reynolds Number.

**Table 4**
Loads and coefficients for the aerodynamic analogy of the tower.

| | |
|---|---|
| Reynolds number for RWT - supercritical region | $5.5{\cdot}10^6$ |
| Reynolds number for prototype tower - subcritical region | $6{\cdot}10^4$ |
| Drag coefficient for RWT tower | ca. 0.56 |
| Drag coefficient for prototype tower | ca.1.2 |
| Drag force on RWT (scaled 1:15) [N] | 10.72 |
| Drag force on prototype [N] | 23.15 |

**Table 5**
Tower characteristics.

| | |
|---|---|
| Outer diameter [m] | 0.18 |
| Thickness [m] | 0.005 |
| Cross-sectional area [m2] | 0.002712 |
| Polar moment of inertia [m4] | $2.02{\cdot}10^{-5}$ |
| First moment of inertia [m4] | $1.01{\cdot}10^{-5}$ |
| Second moment of inertia [m4] | $1.01{\cdot}10^{-5}$ |
| EJ [MPa m4] | $1.8{\cdot}10^6$ |
| Height [m] | 7.5 |
| Linear mass [kg/m] | 19.27 |
| Weight [kg] | 148.17 |

**Table 6**
Actual and target mass of the OSP.

| | Prototype | Target | Error [%] |
|---|---|---|---|
| Tower mass [kg] | 197 | 186.19 | 5.8 |
| Nacelle mass [kg] | 155 | 132.15 | 17.4 |
| Rotor mass [kg] | 106.5 | 67.56 | 57.7 |

### 2.5. Nacelle scaling process

As previously stated, Froude approach was used to scale dimensions and global mass for the nacelle. Although these constraints are

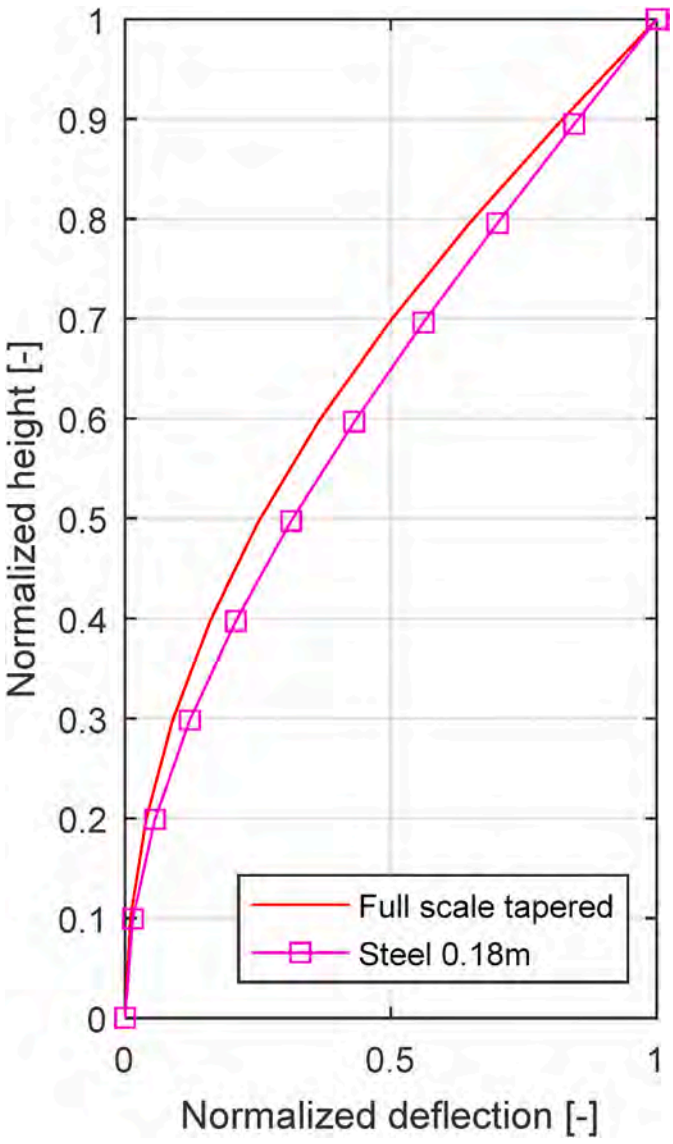


**Fig. 12.** Modal shape comparison between RWT and OSP towers.

**Table 7**
The evaluated design load cases.

| Case Name | U [m/s] | Ω [rpm] | Collective Pitch [°] | Yaw Angle [°] |
|---|---|---|---|---|
| Rated | 5 | 101.9 | 0 | 0 |
| Rated Yaw | 5 | 101.9 | 0 | 30 |
| Park | 33 | 0 | 90 | 0 |
| Full Exposure | 33 | 0 | 0 | 0 |
| Cut-Out | 10.96 | 109.47 | 22.67 | 0 |

important, also functionality criteria must be taken into account in designing the internal components of the nacelle. The following values of mass are obtained at the end of the design process and compared with the target values (Table 6).

It is clear from mass and inertia data that the greatest error is made on the rotor mass scaling. This is due mainly to the rotor hub, which hosts several commercial components like actuators and bearings, and that is designed with the aim of firstly guarantee resistance and stiffness.

### 2.6. Structural design

The OSP presented in this work has to be deployed in an open-sea laboratory, and thus it is at the same time an aeroelastic model and a machine that must resist uncontrolled environmental conditions. Bearing this in mind, the structural design of the model was performed according to the IEC standard (IEC 61400-2:2006), which classifies wind turbines in four classes, depending on the rotor swept area. Class IV collects small wind turbines, with less than 200 $m^2$ rotor-swept area.

Among the 10 load cases suggested by the standard, only the five reported in Table 7 were considered, being the other five deemed not significant in consideration of the project characteristics. Four parameters are adopted to describe each load case: wind speed, rotor rotational speed, blade collective pitch angle, nacelle yaw angle. In the Rated case the machine experiences the maximum thrust force in operating conditions, with a wind speed of 5 m/s. The Park case (H in IEC 61400-2:2006) considers the turbine with blades fully feathered, and the wind speed is set to the maximum one considered in the design. The Full Exposure case is not listed in the IEC 61400-2:2006, and was considered to improve the safety of the entire design. This case considers the wind turbine parked with the blades set at zero pitch angle, that is the condition of maximum blade area projection on the incoming flow direction, and consequently of the maximum aerodynamic load on the structure. For both the Park and Full Exposure cases, the considered wind speed is the 50-year return period wind speed for the test site (33 m/s). Inside each load case, the forces acting on the blades are computed in rigid steady-state simulations in FAST. Relevant outputs considered in the assessment of the turbine components are:

- Rotor power and aerodynamic torque: these loads are distinctive for a wind turbine, expressing the related performances. The rotor power is the power output of the turbine without considering the electrical efficiency while the aerodynamic torque is applied to the main axis due to the rotor rotation. They are used in the main axis actuation design.
- Rotor thrust: it is the force acting on the rotor and transferred to the tower. It is needed for the tower assessments and for the mechanical design of the nacelle components.
- Yaw loads: these are needed in order to design the yaw actuation.
- Root loads: these are the forces acting on the blade root. These loads are needed in order to design the pitch actuation
- Tip deflections: these are the maximum deflections of the blades evaluated at tip. They are needed to assess the capability to avoid any collision between the blades and the tower.

### 2.7. Tower structural design

The tower is a crucial part of a wind turbine due to the structural role

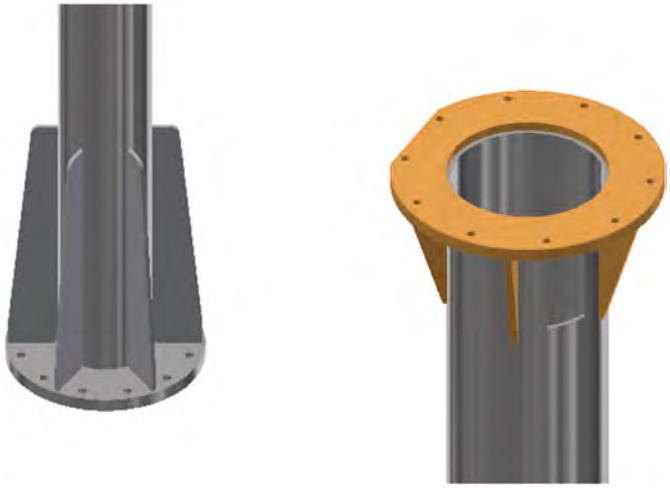

**Fig. 13.** Tower-connection flanges.

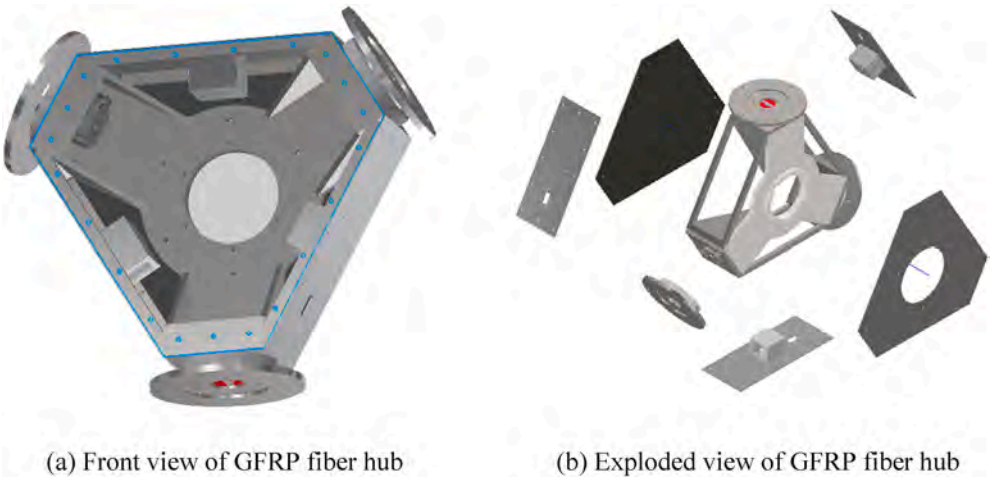


**Fig. 14.** Final design solution for the rotor structure.

that it provides, therefore proper assessments must be carried out. The idea is to consider the worst possible conditions for every analysis, namely the Full Exposure case, because it has the maximum value of thrust. Other load cases are resulting in lower forces on the considered parts. Only for the tower assessment, the effect of the tower drag force on the tower itself was considered.

The whole model, comprising the bottom flange, the tower and the upper flange has been modeled in ABAQUS. Weldings are modeled in their real position and with real dimensions, while the interactions between the tower and flanges are modeled as frictionless, hard surface to surface contacts. The application point for the loads is on the axis of the tower, at the height of the hub. Transport moments are considered for the thrust. The boundary condition at the bottom flange is a clamp, distributed on the holes that will host the bolts fastening the flange to the transition piece. Solid elements are considered for the whole model. A sketch of the top and bottom connections is reported in Fig. 13.

The first assessment is related to the stresses along with the tower, in order to ensure its structural integrity. The entity of stresses along the tower has been evaluated showing values well below the maximum allowable stress for the adopted material. Welded joints connecting the flanges to the tower were also verified. Secondly, the maximum top deflection was considered. This assessment is very important because the deflection can cause collisions between the tower and the blades reducing the gap between the components. From the performed analysis the maximum displacement at the top of the tower turned out to be ≈ 0.1 m in the direction of the upcoming wind. This value related to the tower height is equal to 1.43%: the resulting value is considered acceptable because the percentage deflection for the DTU is 2.5% due to 2.6 m of maximum deflection and 115.63 m of full-scale tower height. Moreover, also considering the maximum tower deflection, the blade-tower gap in survival conditions results to be inside the safety range, and thus the design is validated (see 3.2.2). Finally buckling assessment was performed. Buckling is an instability that leads to structural failure and its assessment plays an important role for thin-walled tubular steel towers. In long members, such as the tower, failure due to buckling will happen before the yield strength is reached. Buckling is a structural instability phenomenon that occurs suddenly, and it is characterized by catastrophic deflections in normal direction compared to the member axis. Even in this case, the assessment is fully positive.

### 2.8. Rotor structural design

The rotor is composed of the hub and the blades. The principal components of the hub are two carbon fiber plates hold together by the flanges that support the blades assemblies. The structure of the rotor assembly presents some challenges related to the mechanical solutions,

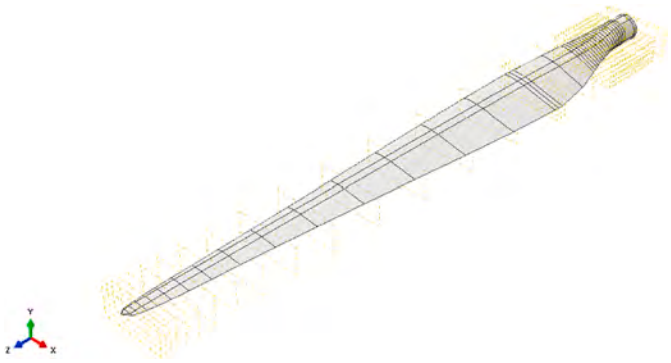

**Fig. 15.** The external geometry of the blade subdivided into 40 blade stations.

mainly due to the mass constraints from the scaling process. The prototype requires technologies that are similar to the ones used in full-size machine and this means that masses and dimensions of some components cannot be reduced as desired. For this reason, the two plates of the assembly (Fig. 14) were designed in glass fiber reinforced plastic (GFRP): the GFRP represents the obvious choice since it can provide nearly the same resistance of steel saving more than one-fourth of the overall weight.

#### 2.8.1. Blade structural design

Blade structural design is the step following their aerodynamic design (see Fig. 15 for the 3D blade shape). The structural project concerns the adoption of the appropriate composite material, the single plies stacking order and the geometric properties of a single ply. Using a FE model. a preliminary structural sizing can be studied in terms of materials and geometry. The idea is to imagine the structure to be composed of discrete parts, 40 sections which are the ones that characterize the FAST model. A good discretization strategy is required in order to simplify the selection of element size and distribution, providing a higher number of sections in the hub region, the one with the biggest variation in terms of cross-section shape. From the maximum chord section to the tip region the blade discretization is coarse because the variation of chord and thickness slows down and becomes linear, so a good refinement can be achieved even with a small number of sections.

In terms of material, fiber reinforced plastics (FRP) were chosen: they are particularly known for their low density, high stiffness and strength therefore they are particularly suitable for wind energy applications, where all three characteristics are of first importance. A composite is a mixture of two or more distinct constituents or phases, where

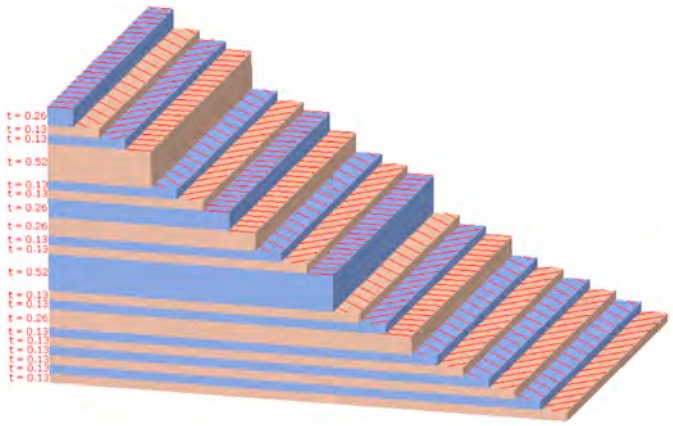

**Fig. 16.** Example of the ply stack plot of the external shell (from r = 0 to r = 0.7718m).

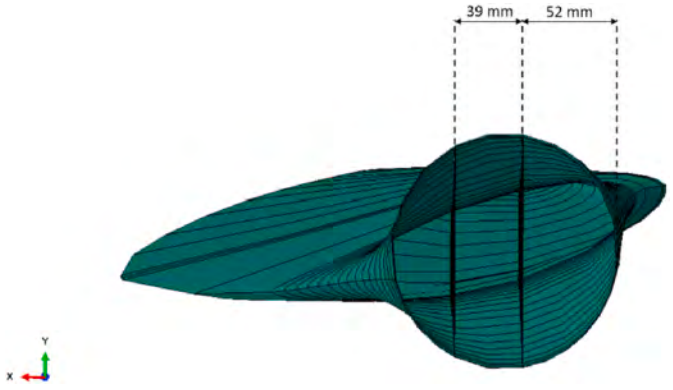


**Fig. 17.** The 3D geometry of the shear webs.

both the materials are present in a reasonable portion and the properties of the two materials are well distinct. FRP are classified according to the kind of reinforcement (fiber) and the matrix (embedding material). In particular, the choice has fallen into using a GFRP (glass fiber reinforced plastic) with an epoxy matrix. Two different kinds of fibers have been selected, the S2-glass UD and the E-glass FABRIC. S2-Glass are classified as high-strength glass fiber because of their level of performance and the one selected is used to produce a unidirectional ply. Thanks to the higher level of silica, ultimate tensile and compressive strength, high-temperature resistance and impact resistance are intensified. E-glass FABRIC is instead alkali-free, particularly suitable for electrical applications, and is one of the most popular for its high strength and stiffness along with the low cost. Given the marine environment, the chemical resistance and the insensitivity to moisture drive the choice as well. Once geometry and material were defined, the structural design was realized defining the lay-up of the external structure and of the internal reinforcements (shear webs). The geometry and lay-ups validation was made simulating on ABAQUS all the load cases reported in Table 7. The tuning was based on variation of the total thickness, fibers orientation, number of layers of each type of material. Then scaling requirements need to be satisfied and so, for each dummy run with a different stacking sequence, the mass, moment of inertia and frequencies of the blades were checked.

The root region is subjected to load transfer from higher radial coordinates, and thus it is characterized by the most intense stress level; the tip is instead not constrained to other parts. Then the ply stack thickness is higher in the root region for mechanical resistance issues, while it is lower and lower as the radial coordinates is increasing. The ply stack in the tip region is chosen to match mass and mass moment of inertia of the blade. An example of the ply stack of the external shell in the root region is reported in Fig. 16. Shear webs (Fig. 17), have a constant thickness and no twist, to minimize the manufacturing complexity.

The load cases considered for the blades structural design are the ones reported in Table 7. From the FAST model of the wind turbine the aerodynamic forces to be applied on the blade are extrapolated. Fig. 18 displays the tangential and aerodynamic loads per unit length for each load case. The normal force is positive in downwind direction and the tangential one is positive in the direction of the peripheral velocity of the blade tip. Gravitational and centrifugal loads were included in ABAQUS, as well as volume forces.

The criterion used to evaluate the stress state in the blade section is the Tsai-Hill criterion, which is applied to ABAQUS results considering the IEC and GL (Germanisch-Lloyd) standards. The prescribed global safety factor is equal to 2.43. The results gathered from all the load cases, summarized in Table 7, showed a large safety factor. Blade buckling is another significant failure mode that must be taken into account, being the blade a thin shell, and so a structure particularly prone to this kind of failure. Buckling is a geometric type of instability: the structure shows a stress-strain level proportional to the applied loads until a critical value is reached, then it shows large deformations. The buckling assessment considered in the ABAQUS model is the linear eigenvalue analysis. The safety factor obtained following the guidelines of the GL standard is 2.76. Sectional loads derived from each one of the considered load cases in Table 7 are applied to the sections of the blade, as well as all the loads transported from the remaining regions from the tip. The bottom part of each section was kinematically coupled to a reference point and clamped. Centrifugal forces were not included in the present analysis and, considering that they reduce the compressive load on each section, the results are on the safe side. All buckling eigenvalues exceed the relative safety factor, so the blade is assessed to buckling failure. Blade-tower clearance was checked as well by investigating the blade deflection, in each load case. The deflection in the worst case is 0.16 m, an acceptable value compared to the hub diameter and below

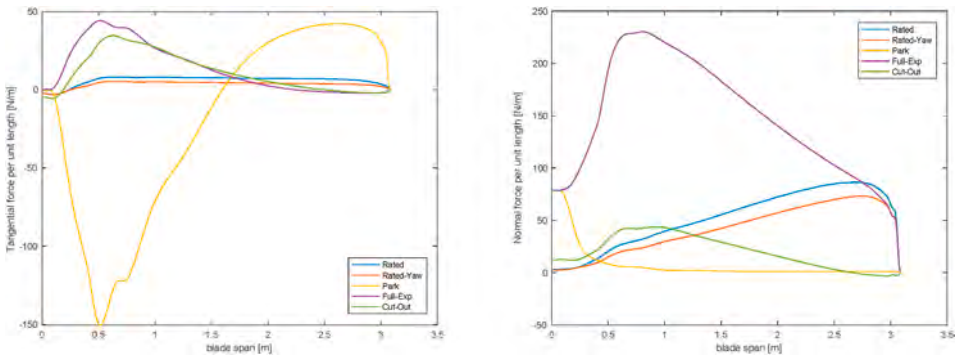


**Fig. 18.** Force per unit length tangential (a) and normal (b) to the rotor plane.

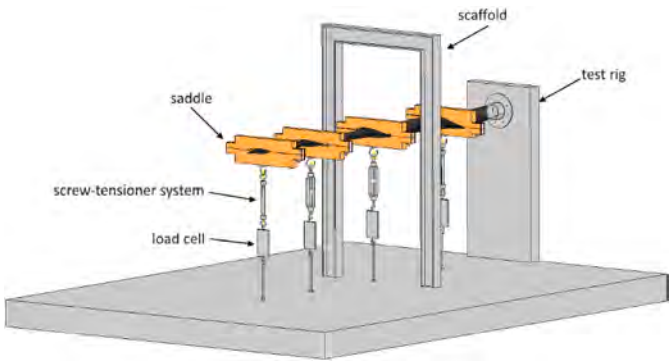


**Fig. 19.** A 3D rendering of the blade test rig.

the minimum blade-tower clearance of 0.47 m. An eigenvalue analysis was instead performed to compute the natural frequencies and mode shapes of the blade, together with the inertial properties (center of mass, moments of inertia). The first flap-wise Froude-scaled natural frequency is 2.36 Hz, while the computed eigenfrequency resulted to be four times higher. This is due to the aerodynamic constraints on the scaling procedure, which forced to have a short blade, with a thin cross-section. Under these assumptions, it is difficult to achieve simultaneously correct natural frequencies and required inertial properties. Nevertheless, the blade mass is close to the target, and even if the blade is much stiffer the result is considered satisfactory, because increased stiffness results in lower deflections and reduced fatigue loads, bringing another time the design on the safe side. Due to the high number of constraints, mainly related to safety issues, that affect the OSP design more than the design of a traditional scale model for laboratory tests, the reproduction of the blade aeroelastic properties was judged less important than properly scaling the global aerodynamic behaviour of the rotor and matching the global masses.

In order to validate numerical calculations, an additional full-scale blade will be manufactured to perform structural resistance tests and modal analysis. Concerning structural tests, the reference standard is the IEC 61400-23:2002 technical standard for full-scale structural testing of wind turbine blades. A short description of the planned tests is reported in the following section.

### 2.8.2. *Blade structural tests description*

Only static structural tests were planned for the blade because, due to the short period of operation of the outdoor prototype, fatigue tests are deemed to be not necessary. The testing procedure is termed in the standard as "load based", meaning that the blade is subjected to the loads found in the design phase, corrected with several coefficients, and it is not voluntarily brought to failure. Five load cases have been considered in the design phase, and the same load cases are chosen to perform the structural tests. The blade is loaded in the spanwise and in the edgewise direction; the radial loads (from gravity or centrifugal force) are not comprised in the testing procedure (Fig. 19 and Fig. 20 (a)). The blade is loaded in a finite set of points to reproduce as much as possible the distribution of stresses coming from the real operational distributed aerodynamic loading. The design loads to be reproduced are multiplied by a suggested load partial safety factor $\gamma_f = 1.35$ (IEC 61400-23:2002). The blade is fixed to a rigid support through the bolted end-flange used to connect it at the hub of the machine ((Fig. 20 (b)). This procedure is suggested by the standard itself to include in the testing phase also the blade root fixing device. The blade is loaded in four points, reported in Table 8, and the amount of spanwise or edgewise force to be exerted is set to reproduce the correct shear force along the blade axis (Table 9) (Fig. 19).

The resultant bending stress is a bit higher than the one found in design, so the setup is conservative.

The heaviest case is the Full Exposure one, and the real and reproduced load conditions are reported in Fig. 21. It is evident that the stair-like shape of load reproduced in tests results, in certain regions, in lower shear stress than the one found in the design phase; however, the locations of load application are chosen so as to have a shear load higher than the design one in the most sensitive areas of the blade (change of lay-up or thickness, minimum safety factor).

The amount of force being exerted is monitored with load cells. The force is transmitted to the blade through a wooden sleeve that prevents local damages of the external blade skin and avoids undesired local stress concentrations. The stress along the blade axis is measured with extensometers. The load is applied for a duration of 10 s, as it is suggested by the standard if the information of peak load duration is lacking.

**Table 8**
Load application points along blade span.

| SectionLoad | Load Span Location [m] |
|---|---|
| 1 | 2.85 |
| 2 | 2.28 |
| 3 | 1.5 |
| 4 | 0.63 |

**Fig. 20.** Static test set-up: (a) Blade structural test bench (b) Blade bolted cap.

**Table 9**
Spanwise (FN) and Edgewise (FT) forces applied during testing.

| SectionLoad | Rated | | Rated-Yaw | | Park | | FullExp | | Cut-Out | |
|---|---|---|---|---|---|---|---|---|---|---|
| | FN | FT | FN | FT | FN | FT | FN | FT | FN | FT |
| | [N] | [N] | [N] | [N] | [N] | [N] | [N] | [N] | [N] | [N] |
| 1 | 57.83 | 3.33 | 48.85 | 1.87 | 0.67 | 27.18 | 54.84 | −1.28 | −1.33 | −1.40 |
| 2 | 72.01 | 6.53 | 57.57 | 3.69 | 1.15 | 19.95 | 124.53 | 2.23 | 4.44 | 1.46 |
| 3 | 115.75 | 11.74 | 93.08 | 6.92 | 2.70 | −7.66 | 262.01 | 19.04 | 27.16 | 13.86 |
| 4 | 98.55 | 13.51 | 77.51 | 7.70 | 10.42 | −79.31 | 326.31 | 35.84 | 38.62 | 25.23 |

The load is applied to the blade through cables stretched by appropriately loaded threaded rods.

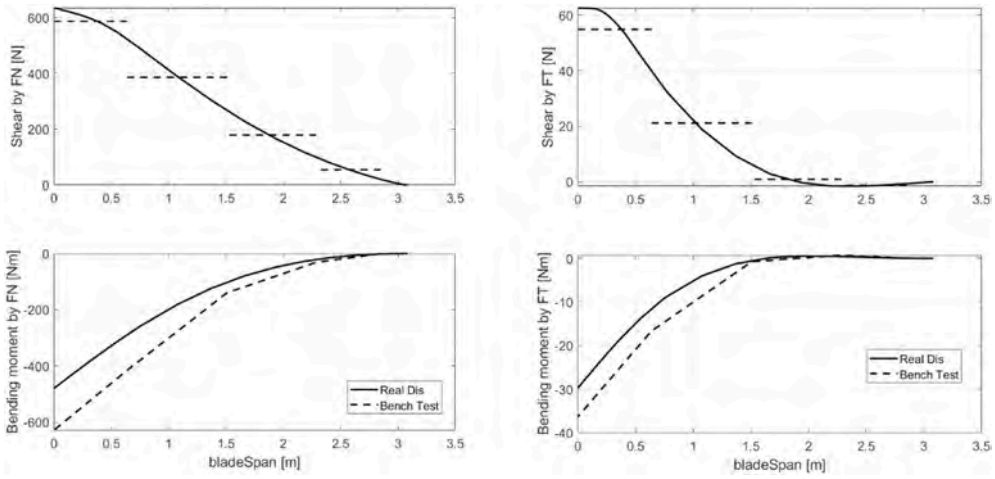


**Fig. 21.** Target and reproduced shear and bending moment along blade span (left: spanwise; right edgewise).

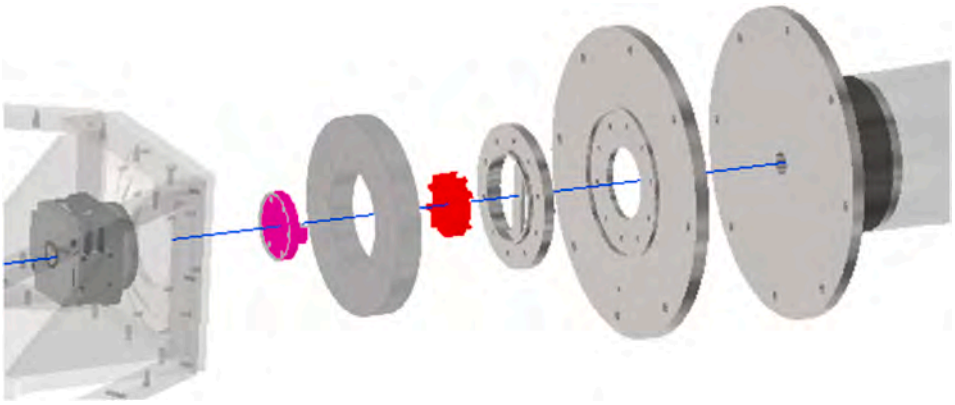

**Fig. 22.** Pitch system assembly.

*2.8.3. Blade assembly and pitch actuation*

The three blades are assembled in order to permit the connection to the hub and to provide the actuation of the pitch DoF. While designing this system the foundation characteristics are: three identical assemblies placed at 120 deg angle span with respect to the rotor axis for a three-bladed wind turbine and Plug & Play specification for each blade in order to guarantee and easy disassemble process of the components. The configuration adopted for the pitch system is displayed in Fig. 22. The motion chain is composed by an actuator connected to an intermediate flange with an Oldham coupling. The flange is mounted on a bearing attached to the rotor hub and it is bolted to the blade cap. The intermediate flange between the blade cap and the assembly allows to easily mount the blades once the rest of the turbine has been already installed in place. The adopted motor is a servo drive with harmonic gearing, so to have a negligible backlash during actuation.

The blade pitch DoF allows the rotation of the blade about its axis. This model is equipped with individual pitch actuation. Pitch actuation is used in normal operation and it is driven by the power controller. It is also used for parking mode and for safety, for example, if it is necessary to perform aero brake for shutdown operation. The load cases reported in Table 7 were used to choose and verify all the components of the blade assembly. In particular, the bearing and the structural components were verified while the actuation system was chosen in order to grant the desired performances in terms of available torque and precision in positioning, together with low mass value and low dimensions. The Oldham coupling was assessed considering the maximum torque and the load conditions of Table 7.

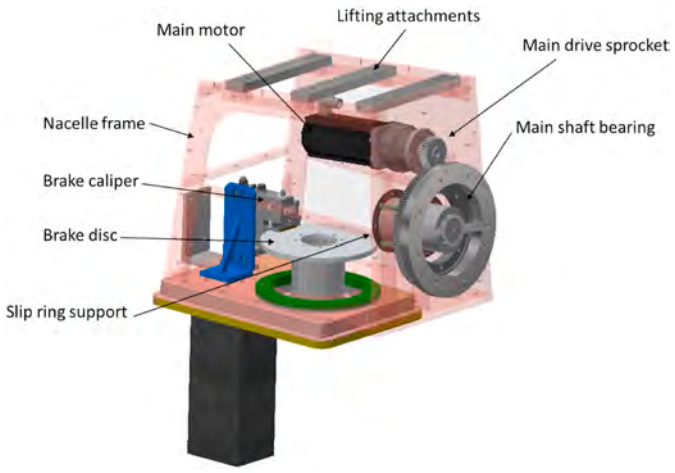


**Fig. 23.** Nacelle assembly components.

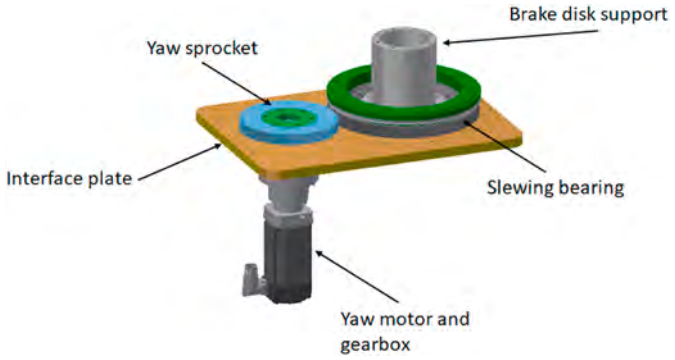


**Fig. 24.** Yaw actuation system.

### 2.9. Nacelle project

The nacelle assembly represents the main structure that supports the rotor and hosts components like the yaw actuator, yaw brake, main motor and gearbox, and slip-ring (see Fig. 23). Guidelines for the design of the nacelle are mainly three:

1. Structural requirements: the nacelle transfers loads from the rotor to the tower and must be designed primarily as a structural component. Moreover, it must protect all the motors and other devices from the external environment and weather conditions. Not only the expected load in operating conditions must be considered at this stage, but also the extreme events.
2. Due to its position on top of the tower, the nacelle mass is affecting the flexible dynamics of the tower, so it must be scaled properly to respect aeroelastic constraints. This is a typical constrain in designing aeroelastic models.
3. It must be a Plug & Play component: the purpose is to ensure an easy installation process and easy accessibility to the internal devices. Installation issues have to be carefully taken into consideration in designing a model for an outdoor laboratory.

The structure of this assembly has been kept as simple as possible and it is made of four steel plates welded together. The front plate supports the rotor slewing bearing and is inclined of 5 deg to guarantee the same rotor tilt of the RWT. The front plate also supports the slip-ring, which is aligned with the rotor axis, for the transmission of power and signals to all the devices comprised in the hub, and the main motor. The lateral steel plates provide structural rigidity to the nacelle structure. The assessment of the nacelle structure is conducted with a FEA in ABAQUS. The loads are applied to the front plate and along the axis of the shaft; the structure is then clamped at the bolt holes of the base plate. The FE analysis to ultimate loads shows a level of stress everywhere below the allowable one so that the design of the frame is validated The nacelle allows the yaw rotation to maintain the rotor plane always oriented perpendicularly to the wind. This is fundamental for a wind turbine deployed in an outdoor laboratory, where the wind direction is variable and not controllable. The yaw DoF is actuated through the coupling between the motor sprocket and the external gear of the slewing bearing selected for this application (a sketch of the yaw actuation system is reported in Fig. 24.).

The actuation system is realized by attaching the motor to the base plate, a solution similar to full-size turbines. The yaw actuator was sized to allow the motion of the rotor-nacelle assembly under the load conditions on the yaw axis founded in the relevant cases reported in Table 7. The slewing bearing is used for motion transmission in addition to supporting the nacelle and rotor assemblies. For this reason, it was selected and verified considering the maximum required torque for the yaw motion among the load cases reported in Table 7. The yaw system is also equipped with a brake that can hold the yaw angle fixed. The yaw brake is of electromagnetic type. The single brake caliper is mounted inside the nacelle assembly on the nacelle base plate and the brake disk is attached to the tower top flange. The disk remains still with respect to the tower and the brake caliper rotates along with the rotor nacelle assembly. The brake capability to hold the rotor nacelle assembly still is assessed considering the same load cases depicted for the yaw drive assessment.

The rotor actuator is required for the turbine normal operation in the whole range of wind velocities. The demanded main motor torque (corresponding to the generator torque on a real machine) is commanded by the wind turbine power controller. This DoF is actuated with the same solution used for the yaw one: a slewing bearing with an external gear coupled with a sprocket, which is connected to the main actuator. The axis of the generator side of the transmission is parallel to that of the rotor. Introducing an offset between the generator and the rotor axis is required to fit a slip-ring in the assembly, since this must be aligned with the rotor axis for cables connection. The power generated during wind turbine operation is dissipated through braking resistors.

## 3. Control strategies

The wind turbine will be featured by a full mechatronic system including actuators, sensors and a control and monitoring systems that allow the model to achieve a multi-megawatt machine range of capabilities. This system can manage the wind turbine in different modes of operation as normal operation, parking or emergency shutdown. The embedded control and monitoring system designed for the model is composed of main and power controller described in the next sections.

### 3.1. Main controller

The main control and monitoring system's task is to manage the different operating modalities of the machine and to deal with fault and emergency procedures. It also manages the sub-controllers (Power controller and Yaw controller), all the communications and data acquisition. The main operating modalities are:

- Normal operation: the turbine works in normal operation under the command of the power controller. If the wind speed is within the power generation range, the power controller operates normally. If the wind speed is below the power generation range, the turbine is ready for start-up. If the wind speed is above the power generation range the machine automatically shuts down.
- Parking: in this modality the turbine is parked in the safest configuration. The yaw axis is still controlled.

- Fault/shut-down: if any fault is detected by the main controller, the operating modes switch to Fault/shut-down and the machine is stopped accordingly to the fault case.

The main controller can be manually operated via wireless/wired communication remotely, and it is also possible to change the operation model interactively.

### 3.2. Power controller

The wind turbine normal operations will be regulated by a power controller. The power controller strategy is a traditional variable-speed variable pitch (VS-VP) and it allows to regulate power through the machine operating range. This is the control strategy generally used in current multi-megawatt turbines. The source of the control logic adopted is the basic DTU Wind Energy Controller (Hansen and Henriksen, 2013) designed for the DTU 10 MW. It was selected for this work in order to reproduce the RWT controller performances. The controller model is developed in MathWorks Simulink environment and its definition will follow. The controller chosen for the wind turbine outdoor scaled prototype follows a traditional region-based scheme. For below-rated wind speeds, the machine works in partial load region: the wind turbine operates at constant blade pitch angle and variable rotor speed, acting on the generator torque set as:

$$Q_G = K_G \omega_G^2 \tag{3}$$

where $K_G$ is the generator torque gain for maximum power coefficient tracking and $\omega_G$ is the generator speed. For above-rated wind speeds, the machine works in full-load region: the wind turbine operates at variable blade pitch angle and constant rotor speed. The controller holds the generator torque constant and the rotor collective pitch angle is adjusted by means of a proportional-integral (PI) controller as follows:

$$\beta = \left(k_P^{\omega} e_{\omega} + k_I^{\omega} \int e_{\omega} dt\right) + \left(k_P^{P} e_P + k_I^{P} \int e_P dt\right) \tag{4}$$

where $e_\omega$ is the rotor speed error and $e_P$ is the power error, $k_P^P$ and $k_I^\omega$ the proportional and integral gains of the speed controller and $k_P^P$ and $k_I^P$ the proportional and integral gains of the power controller. The pitch controller features an additional gain scheduling law. The gain scheduling factor is the product of two terms, the aerodynamic gain scheduling factor and the nonlinear gain scheduling factor. The first one is the aerodynamic gain scheduling and accounts for the different aerodynamic conditions faced by the rotor. The second contribution increases the controller sensitivity to large speed excursions. The formulations are the following:

$$\eta_A = \frac{1}{1 + \frac{\beta}{KK_1} + \frac{\beta^2}{KK_2}} \tag{5}$$

$$\eta_{NL} = 1 + \frac{e_\omega^2}{(\omega_2 - \omega_0)^2} \tag{6}$$

where $KK_1$ and $KK_2$ are the linear and quadratic (if present) aerodynamic gain scheduling coefficients and $\omega_2$ is the speed where pitch controller gains are doubled. Two linear transitions are used to start the wind turbine generator, passing from zero to the optimal mode torque, and to reach Rated conditions from the terminal partial load region.

#### 3.2.1. Controller tuning

The wind turbine controller parameters need to be tuned to properly reproduce the target dynamic behavior of the full-scale wind turbine. The following goals are kept into account in the controller tuning process:

1. Achieve the correct steady-state operating conditions. In particular:
   - Thrust force. The steady-state thrust force developed by the wind turbine affects the dynamic
   - Equilibrium position of the floating system. This is responsible for differences in the mooring line force-displacement characteristic and hydrodynamic loads. The controller, as the DTU reference, is a power controller which aims at regulating the power extraction, minimizing the rotor speed error and thus it's not directly tuned to provide a specific thrust force. However, being the thrust force a key factor in FOWTs, the correct representation of the thrust force is verified for the operating range.
   - Rotor speed, torque and power. Torque and power are among the main performance indexes for any wind turbine. However, the outdoor experimental tests are more focused on the investigation of global FOWT dynamics rather than the optimization of the machine power output. The correct reproduction of speed, torque, and power oscillations may be of some importance.
2. Achieve the correct dynamic response of the controlled system. Being tests focused on global FOWT dynamics it is of fundamental importance to correctly model the response of the controlled system and, mainly, the coupling between platform modes and drivetrain dynamics.
3. Make the controller implementation feasible on the real mechatronic system. Some modifications have to be introduced in order to second limitations from the hardware used to control the model operations.

The parameters are evaluated starting from (Hansen and Henriksen, 2013) where all the controller input data are given. The full-scale parameters are scaled down to model scale according to the scaling law fully described in this work. The controller parameters are listed in Table 10. The parameters are given at model scale and referring to the low-speed shaft. The pitch controller parameters are tuned with the main goal of enabling the model to reproduce the full-scale turbine dynamics. Due to scaling nonidealities, the controller parameters need to be properly tuned for the model. This operation is of fundamental importance since the pitch controller is known to have a great influence on the overall system dynamics.where $K_{\beta Q}$ in the aerodynamic blade pitch to rotor torque sensitivity evaluated at Rated condition, $k_p$ and $k_i$

**Table 10**
VS-VP power controller parameters.

| Parameter | Value |
|---|---|
| Wind speed range [m/s] | 1.754–10.965 |
| Rated rotor power [kW] | 1248.098 |
| Minimum rotor speed [rad/s] | 7.165 |
| Rated rotor speed [rad/s] | 11.464 |
| Minimum pitch angle [deg] | 0 |
| Maximum pitch angle [deg] | 90 |
| Frequency of generator speed filter [Hz] | 2.281 |
| Damping ratio of speed filter [-] | 0.7 |
| Generator control mode | Constant torque |
| Proportional gain of pitch controller [rad/(rad/s)] | 0.0460 |
| Integral gain of pitch controller [rad/rad] | 0.141 |
| Proportional power error gain [rad/W] | 0.0000321 |
| Integral power error gain [rad/(Ws)] | 0.000365 |
| Coefficient of linear term in aerodynamic gain scheduling [deg] | 3.4 |
| Relative speed for double nonlinear gain [-] | 1.3 |
| Time constant of 1st order filter on pitch angle [1/1P] | 0.438 |

$$\omega_0 = \sqrt{\frac{K_{\beta Q} * k_i}{J_R}} \tag{7}$$

$$h = \frac{K_{\beta Q} * k_p}{2 * J_R * \omega_0} \tag{8}$$

To tune the PI pitch controller gains, a 1-DoF model of the pitch-controlled drivetrain is considered. The circular frequency and the damping ratio of the drivetrain are imposed to be equal to the full-scale reference turbine; their expression is the following.

**Table 11**
Relevant quantities for pitch controller tuning.

| | DTU | model |
|---|---|---|
| Rotor inertia [kgm^2] | $1.56{\cdot}10^8$ | 13.1 |
| Pitch to torque aerodynamic sensitivity at Rated [Nm/rad] | $3.86{\cdot}10^7$ | 351.4532 |
| Proportional gain of pitch controller [rad/(rad/s)] | 0.524 | output |
| Integral gain of pitch controller [rad/rad] | 0.141 | output |
| Calculated/imposed drivetrain circular frequency [rad/s] | 0.187 | 2.13 |
| Calculated/imposed drivetrain damping ratio [-] | 0.347 | 0.347 |

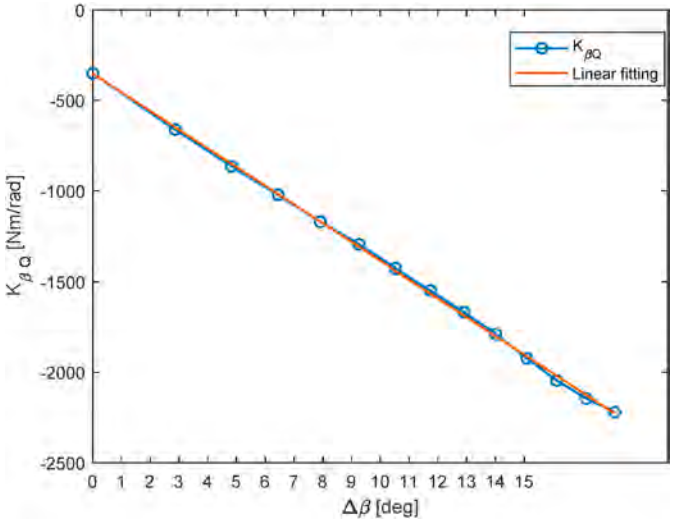


**Fig. 25.** Aerodynamic pitch to torque sensitivity for above-rated operating points and linear fitting.

are the proportional and integral pitch controller gains and $J_R$ is the rotor inertia. Unknown quantities are evaluated by means of FAST numerical simulations both for the model and for the full-scale turbine. The resulting PI pitch controller proportional and integral gains are listed in Table 10 and the other quantities are shown in Table 11. To calculate the aerodynamic gain scheduling coefficients, an interpolation of the aerodynamic blade pitch to rotor torque sensitivity is performed for the model. The aerodynamic blade pitch to rotor torque sensitivity is evaluated by means of FAST numerical simulation for different pitch angles. A linear interpolation is found to be the most suitable. The resulting coefficient is shown in Table 10 and the interpolation in Fig. 25.

### 3.2.2. *Yaw control*

The yaw control has the function of keeping the rotor aligned with the wind direction during operation and, eventually, also during park conditions. It uses as input the wind direction provided by an anemometer placed in the test site. The logic adopted is to keep the rotor yaw DoF still using the yaw brake when the misalignment lay inside a certain threshold. Outside the threshold, the brake is released and the new yaw position is commanded to the yaw drive. The same logic is used also in parking in order to avoid wind excessive wind loads in undesired directions.

## 3.3. *Numerical simulations*

Numerical simulations are performed on the FAST model of the OSP turbine coupled with the Simulink-based controller. For this preliminary assessment, the wind turbine is considered onshore and rigid. In order to assess the controller behavior, the steady-state performances are evaluated. The simulations are performed for wind speed spacing from cut-in to cut-out wind speed, considering constant unsheared wind, fixed and rigid wind turbine model, controlled generator torque and blade pitch, and reaching the steady-state condition for every wind speed. The

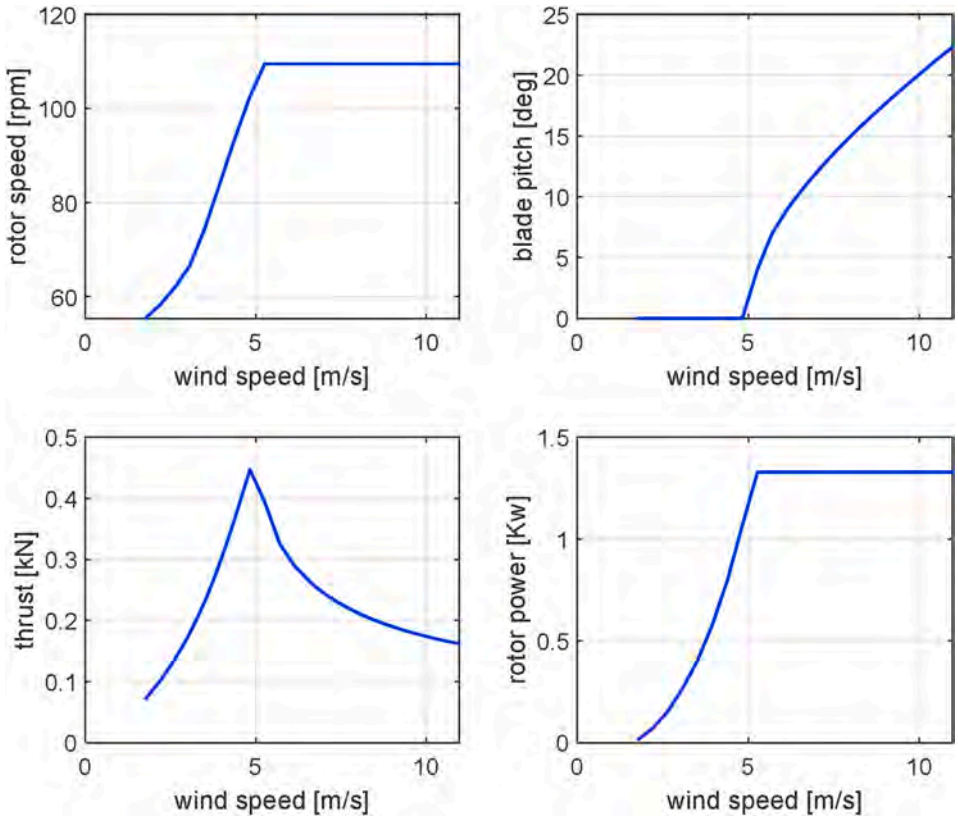


**Fig. 26.** Steady-state performances of the controlled outdoor prototype evaluated in FAST/Simulink: rotor speed, collective blade pitch, rotor thrust and rotor power as function of wind speed.

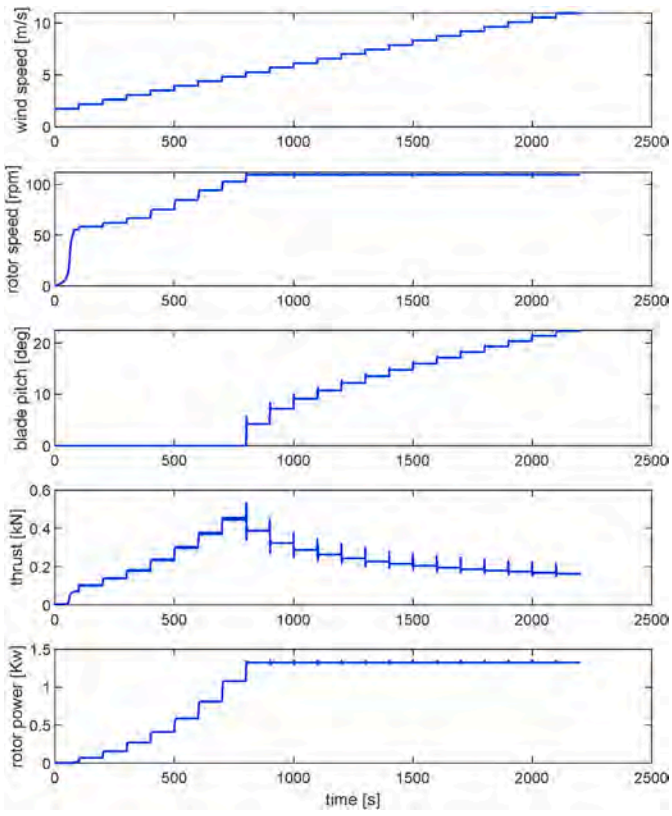


**Fig. 27.** Wind-step test on the controlled outdoor prototype performed in FAST/Simulink.

controller steady-state results are shown in Fig. 26.

The controller behaviour during transients is assessed by performing a wind-step test: starting from cut-in, the wind speed is increased in steps of 1 m/s (at full-scale) every. At the beginning of the simulation the rotor is still, thus simulating also the start-up of the wind turbine. The resulting time histories of rotor speed, collective pitch angle, rotor power and thrust force are presented in Fig. 27. From the rotor speed and blade pitch pictures, it is possible to appreciate how the controller works in the different operating regions. Moreover, comprehensive simulations including OSP platform dynamics and turbine control were performed for relevant load cases within the project activity and no significant interaction were found.

## 4. Conclusion

The present work was developed within the EU H2020 project 'The Blue Growth Farm', which aim is to design a multi-purpose platform for offshore applications, equipped with a wind turbine. In order to reach a TRL (Technology Readiness Level) of about 5–7, experimental activities performed on an intermediate-scale outdoor model were planned. The challenges related to the design of such a large model are presented and discussed, with particular reference to the wind turbine model integrated on the MPP. The typical strategies used for wind turbine models for tests in wind tunnel and wave basin were adapted to the peculiar natural laboratory requirements, integrating the scaling issues with the one related to safety and the structural assessments. A probabilistic approach is used to evaluate wind and wave conditions in the site selected for the tests and these data are used both as input in the aeroelastic design of the tower, in the aerodynamic design of the rotor and for an assessment to extreme events. The machine functionalities were reproduced as in a real wind turbine, trying to match, at the same time, the main requirements of the aeroelastic project as the global masses of the components. Finally, the control strategies are implemented in order to grant the same performances of the RWT properly scaled. The main result of this process is represented by a compromise between different requirements that can give general guidelines in intermediate-scale outdoor model design.

## CRediT authorship contribution statement

**S. Muggiasca:** Methodology, Writing – original draft, Supervision, Conceptualization. **F. Taruffi:** Methodology, Validation, Formal analysis, Writing – original draft, Conceptualization, Software. **A. Fontanella:** Methodology, Validation, Formal analysis, Writing – original draft, Conceptualization, Software. **S. Di Carlo:** Validation, Formal analysis, Writing – original draft, Software, Conceptualization. **H. Giberti:** Conceptualization, Writing – review & editing, Supervision. **A. Facchinetti:** Writing – review & editing, Supervision. **M. Belloli:** Conceptualization, Writing – review & editing, Supervision, Project administration, Funding acquisition.

## Declaration of competing interest

The authors declare that they have no known competing financial interests or personal relationships that could have appeared to influence the work reported in this paper.

## Acknowledgements

This work has been produced in the framework of the Blue Growth Farm project (http://www.thebluegrowthfarm.eu/), which has received funding from the European Union's Horizon 2020 research and innovation programme under Grant Agreement number 774426. The content of the work does not report the opinion of the European Commission and reflects only the views of the author(s), including errors or omissions. The European Commission is also not liable for any use that may be made of the information contained herein.

## References

Bak, C., Bitsche, R., Yde, A., Kim, T., Hansen, M.H., Zahle, F., Behrens, T., 2012. Light Rotor: the 10-MW reference wind turbine. In: Proceedings of EWEA 2012-European Wind Energy Conference. European Wind Energy Association (EWEA).

Bak, C., et al., 2013. The DTU 10-MW Reference Wind Turbine. Technical University of Denmark, DTU Wind Energy, Denmark.

Bayati, I., Belloli, M., Bernini, L., Zasso, A., 2017a. Aerodynamic design methodology for wind tunnel tests of wind turbine rotors. Journal of Wind Engineering and Industrial Aerodynamics 167, 217–227. https://doi.org/10.1016/j.jweia.2017.05.004.

Bayati, I., Belloli, M., Bernini, L., Giberti, H., Zasso, A., 2017b. Scale model technology for floating offshore wind turbines. IET Renewable Power Generation 11 (9), 1120-11.

Bayati, I., Belloli, M., Bernini, L., Boorsma, K., Caboni, M., Cormier, M., Mikkelsen, R., Serdeczny, M., Lutz, T., Zasso, A., 2018a. UNAFLOW project: UNsteady Aerodynamics of FLOating Wind tur- bines. Journal of Physics: Conference Series 1037 (7). http://stacks.iop.org/1742-6596/1037/i=7/a=072037.

Bayati, I., Bernini, L., Zanotti, A., Belloli, M., Zasso, A., 2018b. Experimental investigation of the un- steady aerodynamics of FOWT through PIV and hot- wire wake measurements. Journal of Physics: Conference Series 1037 (5). http://stacks.iop.org/1742- 596/1037/i=5/a=052024.

Belloli, M., Giappino, S., Morganti, S., Muggiasca, S., Zasso, A., 2015. Vortex induced vibrations at high Reynolds numbers on circular cylinders. Ocean Engineering 94. https://doi.org/10.1016/j.oceaneng.2014.11.017, 140-15.

De Ridder, E.J., Otto, W., Zondervan, G.J., Huijs, F., Vaz, G., 2014. Development of a scaled down floating wind turbine for offshore basin testing. Proc. 33rd ASME International Conference on Ocean, Offshore and Arctic Engineering 9A. https://doi.org/10.1115/OMAE2014-23441.

Fontanella, A., Taruffi, F., Muggiasca, S., Belloli, M., 2019. Design methodology for a floating offshore wind turbine large-scale outdoor prototype. In: Proc. 38th ASME International Conference on Offshore Mechanics and Arctic Engineering, Glasgow, Scotland, UK.

Gómez, P., Sánchez, G., Llana, A., Gonzalez, G., 2015. Deliverable D1.1 Oceanographic and Meteorological Conditions for the Design.

Guglielmo, J.J., Selig, 1996. Spanwise variations in profile drag for airfoils at low Reynolds numbers. J M. S.ournal of Aircraft 33 (No. 4).

Hansen, M.H., Henriksen, L.C., 2013. Basic DTU Wind Energy Controller. DTU Wind Energy.

IEC 61400-2, 2006. Wind Turbines - Part 2: Design Requirements for Small Wind Turbines IEC 61400-23:2002 Wind Turbine Generator Systems - Part 23: Full Scale Testing of Rotor Blades, 2002.

Jonkman, J., Butterfield, S., Musial, W., Scott, G., 2009. Definition of a 5-MW Reference Wind Turbine for Offshore System Development Technical Report NREL/TP-500–38060. NREL National Renewable Energy Laboratory.

Jouffray, J.B., Blasiak, R., Norström, A.V., Österblom, H., Nyström, M., 2020. The Blue acceleration: the trajectory of human expansion into the ocean. One Earth 2, 43–54. https://doi.org/10.1016/j.oneear.2019.12.016.

Krieger, A., Ramachandran, G.K.V., Vita, L., Almería, G.G., Berque, J., Aguirre, G., 2015. Deliverable D7.2 Design Basis.

Li, L., Collu, M., Abhinav, A.K., Ruzzo, C., Arena, F., 2019. Analysis of the coupled dynamics of an offshore floating multi-purpose platform, Part A: rigid-body analysis, submitted to international conference on offshore mechanics and Arctic engineering – OMAE2019, Glasgow, UK, 2019.

Li, L., Ruzzo, C., Collu, M., Gao, Y., Failla, G., Arena, F., 2020. Analysis of the coupled dynamic response of an offshore floating multi-purpose platform for the Blue Economy. Ocean Engineering 217. https://doi.org/10.1016/j.oceaneng.2020.107943.

Lyon, C.A., Broeren, A.P., Gigure, P., Gopalarathnam, A., Selig, M.S., 1998. Summary of Low-Speed Airfoil Data, vol. 3. SoarTech Publications, Virginia Beach, VA.

Muggiasca, S., Fontanella, A., Taruffi, F., Giberti, H., Facchinetti, A., Belloli, M., Bollati, M., 2019. Large aeroelastic model of a floating offshore wind turbine: mechanical and mechatronics design. In: ASME 2019 2nd International Offshore Wind Technical Conference, IOWTC 2019. https://doi.org/10.1115/IOWTC2019-7537.

Nassar, W.M., Anaya-Lara, O., Ahmed, K.H., Campos-Gaona, D., Elgenedy, M., 2020. Assessment of multi-use offshore platforms: structure classification and design challenges. Sustainability 12. https://doi.org/10.3390/su12051860.

Pérez-Collazo, C., Greaves, D., Iglesias, G., 2015. A review of combined wave and offshore wind energy. Renewable and Sustainable Energy Reviews 42, 141–153. https://doi.org/10.1016/j.rser.2014.09.032.

Pernice, R., 2009. Japanese urban artificial islands: an overview of projects and schemese for marine cities during 1960s-1990s. J. Archit. Plan. (Transactions AIJ). 74, 1847–1855.

Robertson, A.N., Jonkman, J.M., Goupee, A.J., Coulling, A.J., Prowell, I., Browning, J., Masciola, M.D., Molta, P., 2013. Summary of conclusions and recommendations drawn from the DeepCwind scaled floating offshore wind system test campaign. In: Proc. 32nd ASME International Conference on Offshore Mechanics and Arctic Engineering, Nantes, France.

Ruzzo, C., Failla, G., Arena, F., Collu, M., Li, L., Mariotti, A., 2019. Analysis of the coupled dynamics of an offshore multi-purpose platform, part B: hydro-elastic analysis with flexible support platform, submitted to International Conference on Offshore Mechanics and Arctic Engineering – OMAE2019, Glasgow, UK, 2019.